

XeCl*-laser discharge instabilities at high gas pressures

Z. Harrache, A. Alia, A. Belasri

Abstract. We discuss new features of the XeCl*-laser kinetics by using a detailed analysis of the results of complex computer models. In particular, we consider the development of a high scale instability in a XeCl*-laser discharge. The emphasis is made on fundamental problems, mainly on the limitation of the macroscopic approach to the study of such strongly nonequilibrium systems. The results obtained indicate especially the discharge proprieties at the plasma centre.

Keywords: theoretical modelling, XeCl laser, chemical instability.

1. Introduction

In the last few years it has been established that the limitation of the pulse duration in discharge-pumped XeCl* lasers is caused by the development of microstreamer instabilities in the bulk of the discharge, which are due, in turn, to chemical induced plasma instabilities. This view of the XeCl* discharge is very characteristic, because the usual processes claimed to generate microinstabilities in discharge plasmas are generally of physical nature (e.g., ion-acoustic instabilities, electrode effects, thermal instabilities) [1]. In the case of a XeCl* discharge, the discharge instability seems presently to be due to so-called halogen depletion instability (HDI) [2–6].

This instability mechanism is assumed to result from the following circumstances: (i) electrons in the discharge are mainly destroyed due to dissociative attachment to HCl; (ii) in the XeCl*-laser kinetics there is no mechanism capable of restoring, during laser generation, the HCl molecules destroyed by the dissociative attachment; (iii) the external circuit drives the gap voltage to a self-sustaining quasi-stationary value in order to realise the global balance between the electron density gain and loss in the whole reactor. It follows from statements (i), (ii), and (iii) that the XeCl*-laser discharge is unstable, even with a flat electrode and uniform electric field, with respect to any perturbation of the electron density in a plane normal to

the applied electric field. It is very interesting to observe the local nature of this instability: no instability process seems to take place when estimating only space-averaged quantities, such as the discharge current and voltage. The pioneering work in this field was the one by Coutts and Webb [7], in which the effect of halogen depletion on the local stability of the XeCl* plasma was demonstrated by using a macroscopic approach based on balance equations for HCl concentration. This paper put everything into place, but at the same time it gave rise to a problem of testing the proposed mechanism in the frame of a chemical kinetics scheme that is more realistic than the highly simplified scheme used by Coutts and Webb. For example, the authors of [7] considered only one vibrationally excited level of HCl and ignored many alternative mechanism of HCl destruction in the discharge, such as direct dissociation by impact with electrons or excited Xe atoms. In our previous paper [3], we have shown the importance of upper vibrational levels of HCl for a XeCl*-laser kinetics. Many research works can be found in the literature, concerning the chemical kinetics for the XeCl pumped lasers [8–12].

The present work is a logical continuation of our previously published papers [3–6, 8] in which the chemical kinetics scheme was already developed and confirmed by the results of theoretical and experimental work of Riva et al. [9]. The goal of the present paper is a detailed study, under inhomogeneous conditions, of the volume instabilities at the discharge centre for which the existence of these instabilities has been already demonstrated [5].

2. Model description and kinetic equations

The main purpose of the model is to describe the discharge nonuniformities which are responsible for some limitations of the excimer laser efficiency [13, 14]. Obviously, a uniform discharge (or zero dimensional) model cannot be used to predict the spatial nonuniformities in the excimer active medium. The representation by a resistance network in parallel [15] is required to study these nonuniformities on a high scale. In this network, each of these resistances is described by using a zero dimensional model [16–20]. The network is in perpendicular direction to the discharge axis and is in fact constituted by the juxtaposition of a set of zero dimensional models [3, 5].

In this model, the surface of the discharge is divided ideally into a resistances network in parallel, characterised, as in the case of the zero dimensional model [17], by independent chemical kinetics and a time dependent resistance. This resistance is given by the formula:

$$R = \frac{d}{S\mu en_c}, \quad (1)$$

Z. Harrache Grupo de Espectroscopía de Plasmas, Edificio A.Einstein, Campus de Rabanales, Universidad de Córdoba, E-14071 Córdoba, Spain; Laboratoire de Physique des Plasmas, Matériaux Conducteurs et leurs Applications, Université des Sciences et de la Technologie d'Oran, Oran, 1505 El-Mnaouer, Algérie;

A. Alia Laboratoire de Mécanique de Lille, UMR CNRS 8107, Université des Sciences et Technologies de Lille, 59655 Villeneuve d'Ascq Cedex, France;

A. Belasri Laboratoire de Physique des Plasmas, Matériaux Conducteurs et leurs Applications, Université des Sciences et de la Technologie d'Oran, Oran, 1505 El-Mnaouer, Algérie

Received 3 September 2011; revision received 10 January 2012
Kvantovaya Elektronika 42 (4) 304–309 (2012)
Submitted in English

where S is the surface element (for simplicity, all resistances are supposed to have equal surfaces); d is the gap distance; μ is the electron mobility; e is the electron charge; and n_e is the electron density. Thus, the plasma equivalent resistance for a given time, used in the external circuit equations, has the form

$$R_{\text{eq}} = \left(\sum \frac{1}{R} \right)^{-1}. \quad (2)$$

The electron density in each element of plasma is calculated, as in the zero dimensional model, by solving the Boltzmann equation coupled to the heavy species kinetics and electric circuit equations [4]. Electron–molecule reactions, which have been taken into account, are presented in [3, 8].

For each plasma element it is necessary to solve a set of twenty-one kinetic equations for the discharge species: electrons, NeXe^+ , Ne^+ , Cl^- , Xe_2^+ , Ne_2^+ , Xe^* , Ne^* , Xe_2^* , Ne_2^* , Cl_2^* , NeCl^* , XeCl^* , Xe_2Cl^* , Cl_2 , HCl_0 , HCl_1 , HCl_2 , HCl_3 , $h\nu_{308}$, $h\nu$.

The electron density in a plasma element is obtained by solving the equation

$$\frac{dn_e(t)}{dt} = S_e^+(t) - S_e^-(t), \quad (3)$$

where $S_e^+(t)$ and $S_e^-(t)$ are the electron production term and the electron loss term due to the dissociative attachment, recombination and electron quenching, respectively. The expressions for these terms have the form

$$\begin{aligned} S_e^+(t) &= [\text{Xe}]n_e k_i + [\text{Ne}]n_e C_1 + [\text{Xe}^*]n_e k_i^* + [\text{Ne}^*]n_e C_2 \\ &+ [\text{Xe}^*][\text{Xe}^*]C_3 + [\text{Xe}_e^*][\text{Xe}_2^*]C_4 + [\text{Ne}^*][\text{Xe}]C_5 \\ &+ [\text{Cl}^-][\text{Cl}^-]C_6 + [h\nu_{308}]\{[\text{Xe}^*]C_7 + [\text{Xe}_2^*]C_8\} \\ &+ [\text{Cl}^-]C_9 + [\text{Xe}_2\text{Cl}^*]C_{10}, \\ S_e^-(t) &= n_e \{ [\text{HCl}_0]k_{a0} + [\text{HCl}_1]k_{a1} + [\text{HCl}_2]k_{a2} \\ &+ [\text{HCl}_3]k_{a3} \} + [\text{NeXe}^+]n_e r_1 + [\text{Xe}_2^+]n_e r_2 \\ &+ [\text{Ne}_2^+]n_e C_{11} + n_e \{ [\text{Cl}_2]C_{12} + [\text{Cl}_2^*]C_{13} \}, \end{aligned}$$

where k_i and k_i^* are, respectively, the ionisation rate of xenon and metastable xenon atoms in collisions with an electron; k_{a0} , k_{a1} , k_{a2} and k_{a3} are the rates of dissociative attachment of an electron to a molecule in the vibration state with $v = 0, 1, 2, 3$, respectively; r_1 and r_2 are the recombination rates between electrons and NeXe^+ and between electrons and Xe_2^+ . These rates were tabulated as a function of the electric reduced field E/N using a numerical solution of the Boltzmann equation [21, 22]. The values of constant rates C_{1-13} are 9×10^{-19} , 1.3×10^{-8} , 5×10^{-10} , 3.5×10^{-10} , 1.8×10^{-11} , 2×10^{-6} , 1.8×10^{-9} , 4.2×10^{-7} , 6×10^{-7} , 7.8×10^{-7} , 2.5×10^{-8} , 1×10^{-10} and $3 \times 10^{-7} \text{ cm}^3 \text{ s}^{-1}$, respectively. We assume that all Xe^+ ions can be transformed immediately into NeXe^+ [8]. It is worth noting that although the electronic reaction rates found in the literature show that most references are old, they are still widely used as a basis of the set of models used for description of excimer lasers and lamps [8, 23–25] and plasma display panels [26].

3. Results and discussion

3.1. Model validity

In order to check the validity of the present model, we have compared it with the theoretical work of Longo et al. [27], using the same discharge parameters as those in Ref. [27] (see Fig. 1). Figure 2 shows the comparison of our results with

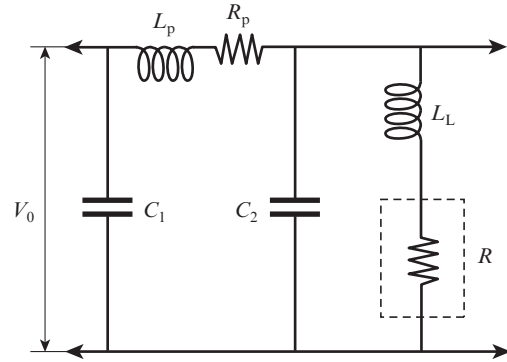


Figure 1. Scheme of the electrical pump circuit: $V_0 = 55 \text{ kV}$, $C_1 = 640 \text{ nF}$, $C_2 = 2.4 \text{ nF}$, $L_p = 63 \text{ nH}$, $L_L = 10 \text{ nH}$, $R_p = 38 \text{ m}\Omega$; the interelectrode gap is $d = 10 \text{ cm}$; the electrode area is $A = 1000 \text{ cm}^2$; the total pressure is $p = 3 \text{ atm}$ (at 300 K); the gas mixture composition is $\text{Ne}:\text{Xe}:\text{HCl} = 99.5:0.44:0.06\%$.

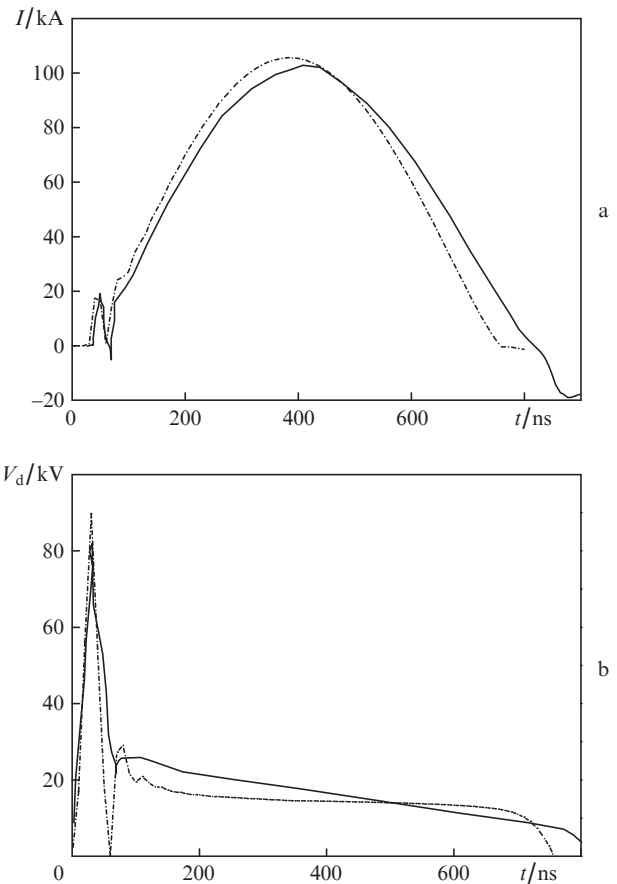


Figure 2. Time dependences of the discharge current (a) and voltage V_d (b) obtained in [27] (solid curves) and in the present work (dash-and-dot curves) under the same condition as in Fig. 1 and at the initial electron concentration $n_e(t=0) = 10^{10} \text{ cm}^{-3}$.

those obtained by Longo et al. [27] using a more sophisticated model, based on solving the Boltzmann equation coupled with more complete chemical kinetics equations. One can see from Fig. 2a that the waveforms and the magnitudes of the discharge current are in agreement. The current peak obtained from our numerical model is slightly higher than that presented in [27]. The temporal variation of the voltage pulse obtained from our model is similar to that of paper [27]. The value of the voltage in the plateau calculated by the model of Longo et al. [27] is close to that of our calculus (Fig. 2b). Figure 3 presents the time evolutions of the concentrations of $\text{HCl}(v=0, 1)$, electrons and metastable xenon for both models. One can see an agreement in the order of magnitudes and their profiles. However, these comparison results can be interpreted only from a qualitative point of view. For quantitative comparisons, the cross sections and the rates must be defined correctly as function of the experimental conditions.

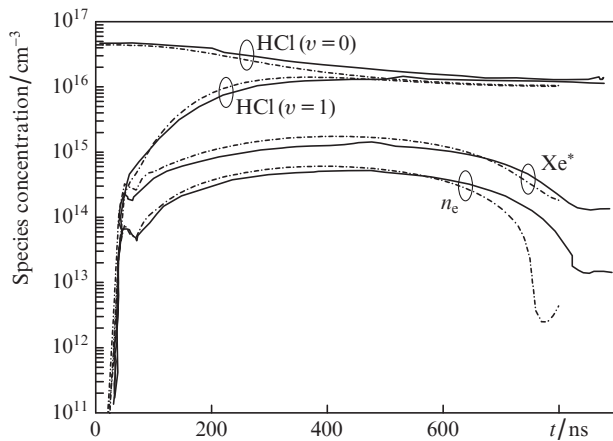


Figure 3. Time dependences of the discharge species concentrations obtained in [27] and in the present work under the same conditions as in Fig. 1 and at $n_e(t=0) = 10^{10} \text{ cm}^{-3}$.

3.2. Some characteristics of chemical instability

We discuss in this section some discharge parameters under inhomogeneous preionisation conditions. The spatial nonuniformities of a high-pressure electrical discharge in a Ne–Xe–HCl excimer gas mixture are presented in Refs [3, 4]. The assumed scheme for the electrical pump circuit is shown in Fig. 4. For the phototriggered laser, at a time t , the capacitor is supposed to be charged, and the discharge is assumed to be instanta-

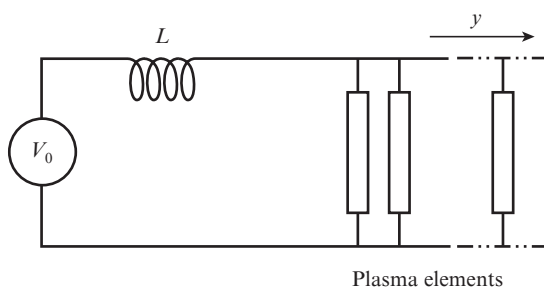


Figure 4. Scheme of the electrical pump circuit used in the present work (y is the transverse distance from the centre to the plasma element). The electrical parameters are given in the text.

neously phototriggered. The parameters of the electrical discharge circuit are as follows: capacity, $C = 150 \text{ nF}$; inductance, $L = 5 \text{ nH}$. The electrodes are plane and rectangular, with dimensions $3 \times 100 \text{ cm}$, and the distance between them is 3 cm . The plasma is represented by some elements in parallel, spaced by 3 cm from each other. The gas mixture composition is Ne:Xe:HCl = 99.33:0.5:0.17%. The total pressure is 3 atm and the applied voltage is 30 kV . Figure 5 presents the temporal variation of the global electrical behaviour of the discharge (discharge current and voltage, voltage across the capacity). This behaviour for uniform (for fluctuations $n_e \leq 10^{10} \text{ cm}^{-3}$) and nonuniform preionisation is slightly affected by the large-

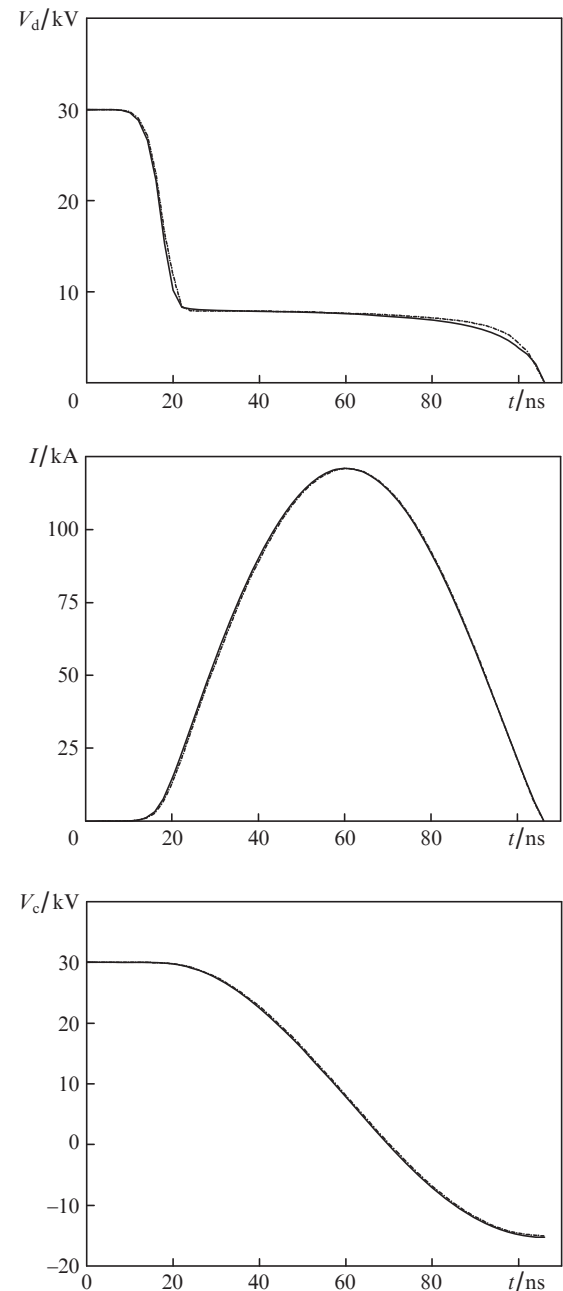


Figure 5. Temporal variations of the discharge voltage V_d , discharge current I , and voltage V_c across the capacitor of the external circuit under the same conditions as in Fig. 4 in the case of nonuniform (solid curves) and uniform (dash-and-dot curves) preionisation density [$n_e(t=0) = 10^{10} \text{ cm}^{-3}$].

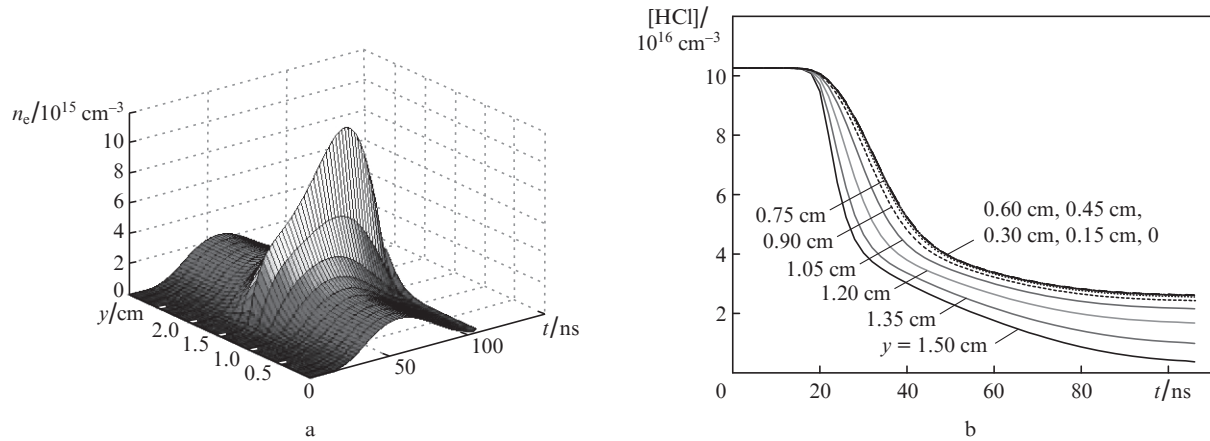


Figure 6. (a) Spatiotemporal evolution of the electron density under the same conditions as in Fig. 4 and (b) temporal variation of the HCl($v=0$) concentration in each plasma element for a charging voltage of 30 kV and a gas pressure of 3 atm.

scale nonuniformities [5]. Figure 5 also clearly shows the local nature of this instability that takes place in a XeCl excimer laser discharge. In Fig. 6a, we plotted the variation of the electron density as a function of time and transverse distance (parallel to the electrode in the direction of the initial nonuniformity). This density is high in the plasma centre (about $1 \times 10^{16} \text{ cm}^{-3}$). The decrease in the concentration of HCl molecules at the vibration level $v=0$ in different plasma elements is shown in Fig. 6b. The halogen concentration is minimal

in the plasma centre (decreases by about 88% at the pulse end), where the electron density is the highest. The concentration decreases by 28 times passing during the time interval $0 \leq t \leq 106 \text{ ns}$.

3.3. Parametric study

Let us now investigate the plasma centre properties using the parallel resistor network model (PRN) including the instability.

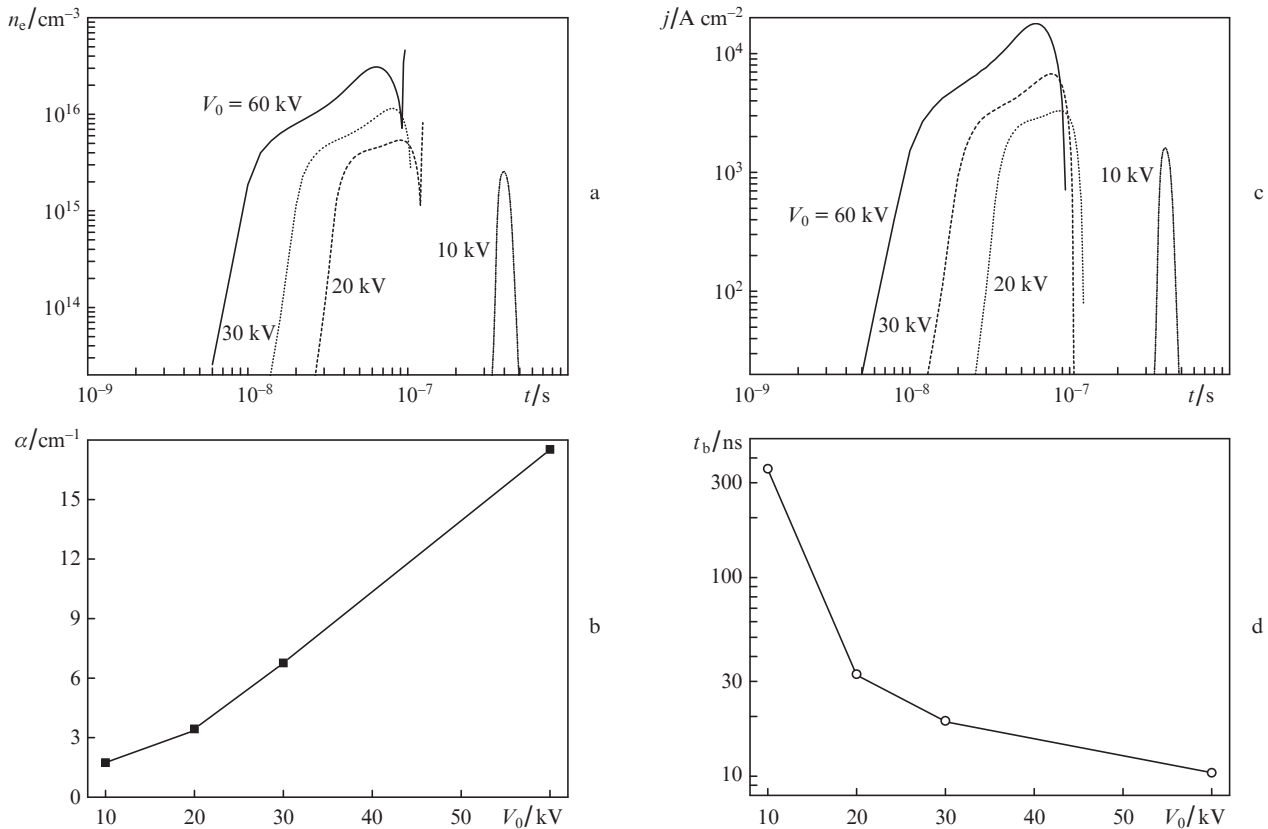


Figure 7. Time dependences of the electron density (a) and current density j (c) for different values of the applied voltage V_0 as well as the dependences of the laser gain (b) and delay time before the breakdown t_b (d). The gas mixture is Ne: Xe: HCl = 99.33:0.5:0.17% and the total pressure is 3 atm.

Namely, we discuss the dependence of the plasma proprieties at the centre on the amplitude of the applied voltage, the gas mixture, and the total gas pressure.

We first investigate the effect of the applied voltage V_0 on the plasma properties and the photon emission in the excimer discharge. It is known that increasing V_0 increases light emission due to an increase in energy deposition. A higher fraction of power deposition goes into producing excitation and ionisation, when the applied voltage magnitude is increased. The effect of the applied voltage on the electron density and the laser gain, during the discharge pulse at the centre ($y = 1.5$ cm), and in the case of a total gas pressure of 3 atm and a gas mixture of Ne:Xe:HCl = 99.33:0.5:0.17% is plotted in Figs 7a

and b. One can see that the electron density and the laser gain increase with increasing V_0 . The dependence of the current pulse on the value of the applied voltage in the plasma centre is shown in Fig. 7c. We can clearly see an increase in the current peak when the breakdown occurs on short times. Figure 7d illustrates the delay time to breakdown as a function of the applied voltage. One can see that the delay time decreases with voltage [8, 17]. In this case, for $V_0 = 10$ kV the delay time is in the order of ~ 350 ns, and at the highest applied voltage it is about 10 ns.

It is known that the electron dissociative attachment to halogen molecules is considered as the dominant electron loss process in the Ne–Xe–HCl laser mixture. Therefore the halogen concentration in the mixture influences strongly the balance between electron production and loss. The time dependence of the current density at the plasma centre, and for the different halogen concentration in the gas mixture (0.01%, 0.05%, 0.17%, and 0.5%) is demonstrated in Fig. 8a in the case of a total gas pressure of 3 atm and an applied voltage of 20 kV. A current profile deformation is observed, with a strong increase in the intensity at the pulse end for the high halogen concentration [3, 28, 29]. For low HCl concentration (0.01%), a decrease in attachment to HCl leads to an increase in the electron density and, therefore, the breakdown occurs on short times (see Fig. 8b). The growth of the HCl concentration at a fixed xenon concentration leads to the reduction of the electron density due to the increase in the attachment to

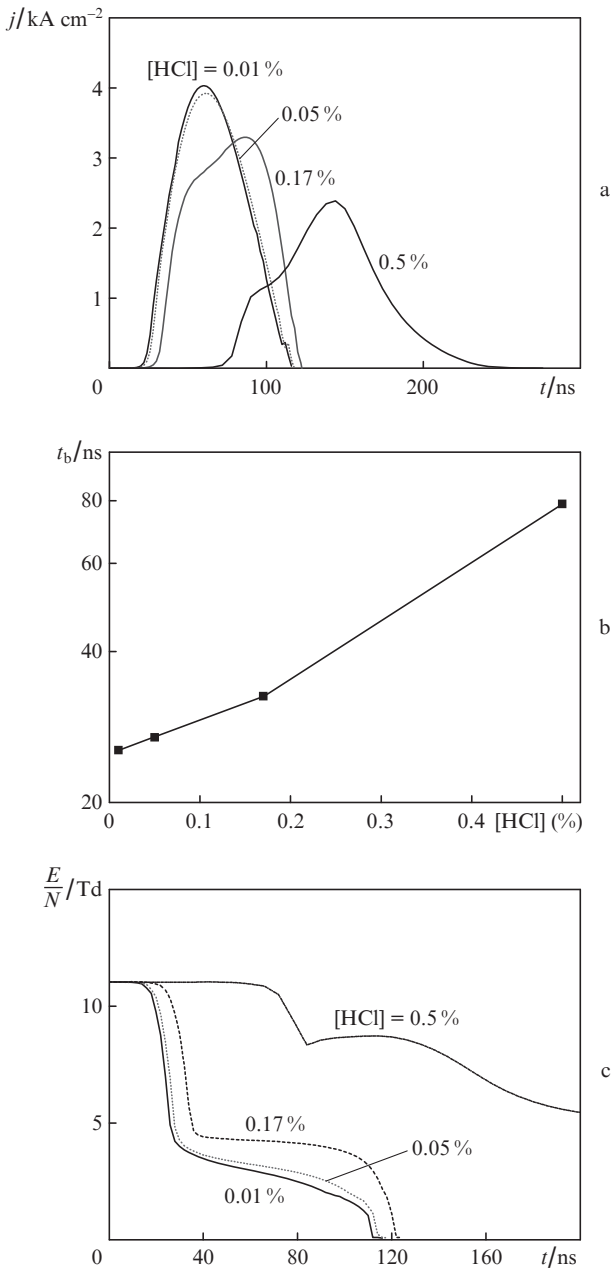


Figure 8. Time dependences of the current density j (a) and reduced electric field voltage E/N (c) for different concentrations of HCl in the mixture as well as the dependence of the delay time before the breakdown t_b on the percentage of halogen in the Ne–Xe–HCl mixture (b). The gas pressure is 3 atm and the applied voltage is 20 kV.

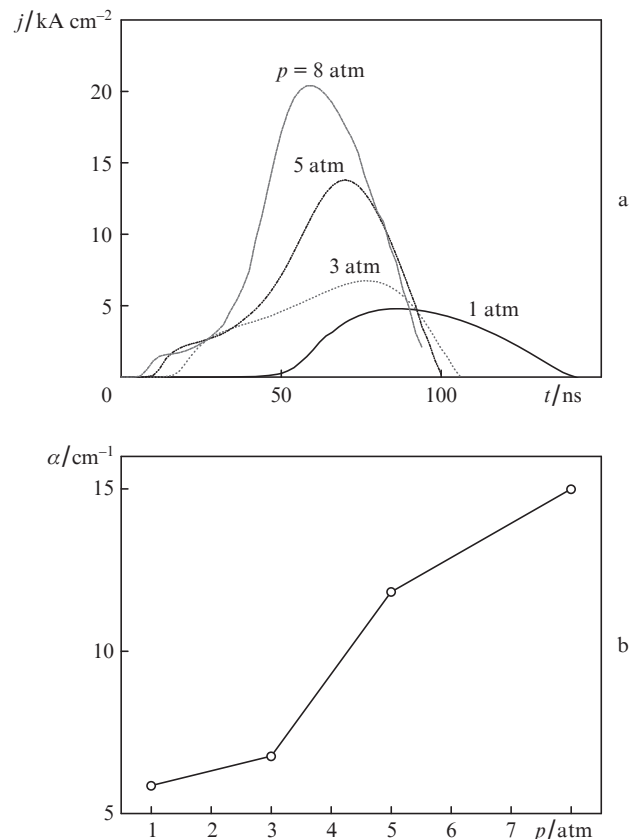


Figure 9. Time dependences of the current density j for different values of the total gas pressure p (a) and the dependence of the laser gain α on the mixture pressure (b). The gas mixture is Ne: Xe: HCl = 99.33:0.5:0.17% and the applied voltage is 30 kV.

HCl and consequently to the increase in the electric field (Fig. 8c).

By taking into consideration the order of the gas pressure's range used in some experimental works, we studied the effect of the gas pressure growth on the discharge properties at the centre, under the same conditions as those in Section 3.2. It is instructive to note that the higher pressure increases the voltage at which the discharge breakdown occurs, thereby increasing the power deposited in the discharge. Figure 9a presents the time variation, during the discharge pulse, of the discharge current density at the centre. It shows a well-pronounced dependence on the gas pressure. The current density at the plasma centre increases with the gas pressure to reach a maximum value of 20.4 kA cm⁻² for a pressure $p = 8$ atm. The variation of the laser gain against the gas pressure is plotted in Fig. 9b. Passing from pressure 1 to 8 atm, the laser gain increases by nearly three times.

4. Conclusions

This work presents an electric and kinetic approach to the study of the development and amplification of the macroscopic instabilities in the Ne–Xe–HCl mixture. These instabilities arise due to an inhomogeneous preionisation and are amplified by the kinetics of the laser medium. The main attention is attracted to the plasma properties at its centre, which can be caused by transition to the arc regime. The study was performed by using a one-dimensional model based on the parallel resistor network concept, consisting in dividing the discharge volume into plasma elements which are connected in no way but through their contribution to the total resistance of the plasma, as seen by the pump circuit. The model, including the plasma chemistry module, the circuit module and the Boltzmann equation module, investigates the electrical and physical characteristics of a high-pressure discharge.

The results predict that under the typical conditions of the discharge at the plasma centre, the increase in the gas mixture pressure and the applied voltage amplifies any nonuniformity. Also, the halogen concentration plays an essential role in the development of nonuniformities.

Finally, the model calculations have shown that the concept of volume instability, with realistic chemical parameters and initial electron density perturbations, is quantitatively unable to explain the difference between theoretical and experimental pulse lengths for large-volume devices, leaving as the only explanation of the discrepancy, the development of a microstreamer instability in the discharge plasma.

Acknowledgements. The authors are grateful to the reviewer for comments and suggestions, which helped to improve the paper. Z. Harrache wishes also to express his thanks for valuable discussions with Yazid Harrache from the USTO University (ALGERIA).

References

1. Longo S., in *Gas Lasers – Recent Developments and Future Prospects* (Boston: Kluwer Acad. Publ., 1996) pp 163–183.
2. Demyanov A.V., Kochetov I.V., Napartovich A.P., Capitelli M., Longo S. *Kvantovaya Elektron.*, **22**, 673 (1995) [*Quantum Electron.*, **25**, 645 (1995)].
3. Belasri A., Harrache Z., Baba-Hamed T. *Phys. Plasmas*, **10**, 4874 (2003).
4. Harrache Z., Belasri A. *Europhys. Lett.*, **66**, 76 (2004).

5. Belasri A., Harrache Z., Baba-Hamed T. *Plasma Devices Oper.*, **12**, 39 (2004).
6. Harrache Z., Amir Aid D., Mehdaoui L., Belasri A. *J. Tech. Phys.*, **49**, 3 (2008).
7. Coutts J., Webb C.E. *J. Appl. Phys.*, **59**, 704 (1986).
8. Harrache Z., Calzada M.D., Belasri A. *Plasma Phys. Rep.*, **37**, 904 (2011).
9. Riva R., Legentil M., Pasquiers S., Puech V. *J. Phys. D: Appl. Phys.*, **28**, 856 (1995).
10. Stielow G., Hammer T., Böttcher W. *Appl. Phys. B*, **47**, 333 (1988).
11. Bychkov Y.I., Yampolskaya S.A., Yastremsky A.G. *Laser Part. Beams*, **21**, 233 (2003).
12. Bychkov Y.I., Yampolskaya S.A., Yastremsky A.G. *Kvantovaya Elektron.*, **40**, 28 (2010) [*Quantum Electron.*, **40**, 28 (2010)].
13. Taylor R.S. *Appl. Phys. B*, **41**, 1 (1986).
14. Osborne M.R., Hutchinson M.H.R. *J. Appl. Phys.*, **59**, 711 (1986); Osborne M.R. *Appl. Phys. B*, **45**, 285 (1988).
15. Kushner M.J., Pindroh A.L., Fisher C.H., Znotins T.A., Ewing J.J. *J. Appl. Phys.*, **57**, 2406 (1985); Kushner M.J., in *Non-Equilibrium Processes in Partially Ionized Gases, NATO ASI Series* (New York: Plenum Press, 1990) Vol. 220, p. 63.
16. Belasri A. *PhD Thesis* (Université Paul Sabatier de Toulouse, France, 1993).
17. Harrache Z., Belasri A. *J. Plasma Phys.*, **73**, 613 (2007).
18. Luck H., Loffhagen D., Botticher W. *Appl. Phys. B*, **58**, 123 (1994).
19. Lamrous O., Gaouar A., Yousfi M. *J. Appl. Phys.*, **79**, 6775 (1996).
20. Turner M.M., Smith P.W. *IEEE Trans. Plasma Sci.*, **19**, 350 (1991).
21. Morgan W.L., Penetrante B. *Comput. Phys. Commun.*, **58**, 127 (1990).
22. Morgan W.L., Boeuf J.P., Pitchford L.C. *The Siglo Database, CPAT and Kinema Software (1995–1998)*; <http://www.siglo-kinema.com>.
23. Belasri A., Khodja K., Bendella S., Harrache Z. *J. Phys. D: Appl. Phys.*, **43**, 445202 (2010).
24. Belasri A., Harrache Z. *Phys. Plasmas*, **17**, 123501 (2010).
25. Belasri A., Harrache Z. *Plasma Chem. Plasma Process.*, **31**, 787 (2011).
26. Benstâali W., Belasri A. *IEEE Trans. Plasma Sci.*, **39**, 1460 (2011).
27. Longo S., Gorse C., Capitelli M. *IEEE Trans. Plasma Sci.*, **19**, 379 (1991).
28. Bahr M., Botticher W., Choroba S. *IEEE Trans. Plasma Sci.*, **19**, 36 (1991).
29. El-Habachi A., Shi W., Moselhy M., Schoenbach K.H. *J. Appl. Phys.*, **88**, 3220 (2000).